Surface Floating 2D Bands in Layered Nonsymmorphic Semimetals: ZrSiS and Related Compounds

Andreas Topp,[1,*] Raquel Queiroz,[2,1,†] Andreas Grüneis,[1,3] Lukas Müchler,[4] Andreas W. Rost,[1,7] Andrei Varykhalov,[5] Dmitry Marchenko,[5] Maxim Krivenkov,[5] Fanny Rodolakis,[6] Jessica L. McChesney,[6] Bettina V. Lotsch,[1] Leslie M. Schoop,[1] and Christian R. Ast[1]

[1]*Max-Planck-Institut für Festkörperforschung, Heisenbergstrasse 1, D-70569 Stuttgart, Germany*
[2]*Department of Condensed Matter Physics, Weizmann Institute of Science, Rehovot 76100, Israel*
[3]*Institute for Theoretical Physics Vienna University of Technology, A-1040 Vienna, Austria*
[4]*Department of Chemistry, Princeton University, Princeton, New Jersey 08544, USA*
[5]*Helmholtz-Zentrum Berlin für Materialien und Energie, Elektronenspeicherring BESSY II, Albert-Einstein-Straße 15, 12489 Berlin, Germany*
[6]*Argonne National Laboratory, 9700 South Cass Avenue, Argonne, Illinois 60439, USA*
[7]*SUPA, School of Physics and Astronomy, University of St Andrews, North Haugh, St Andrews, Fife KY16 9SS, United Kingdom*

(Received 31 August 2017; revised manuscript received 3 November 2017; published 28 December 2017)

In this work, we present a model of the surface states of nonsymmorphic semimetals. These are derived from surface mass terms that lift the high degeneracy imposed on the band structure by the nonsymmorphic bulk symmetries. Reflecting the reduced symmetry at the surface, the bulk bands are strongly modified. This leads to the creation of two-dimensional floating or unpinned bands, which are distinct from Shockley states, quantum well states, or topologically protected surface states. We focus on the layered semimetal ZrSiS to clarify the origin of its surface states. We demonstrate an excellent agreement between density functional theory calculations and angle-resolved photoemission spectroscopy measurements and present an effective four-band model in which similar surface bands appear. Finally, we emphasize the role of the surface chemical potential by comparing the surface density of states in samples with and without potassium coating. Our findings can be extended to related compounds and generalized to other crystals with nonsymmorphic symmetries.

DOI: 10.1103/PhysRevX.7.041073 Subject Areas: Condensed Matter Physics

I. INTRODUCTION

Surface states have gained significant interest as they reflect both surface details and bulk properties. In view of the current search for nontrivial topology in band insulators [1–6] and semimetals [7–14], it has become crucial to characterize different types of surface states which may emerge in these systems. Specifically, it is important to distinguish surface states which reflect surface chemistry, such as dangling bond states [15] or quantum well states [16], from surface states that arise from bulk band topology. Shockley and Tamm states are the most common examples of surface states [17], arising as an additional solution of the Hamiltonian at the interface within a projected band gap. The additional requirement of a band inversion implies a nontrivial band topology even in the absence of spin-orbit coupling (SOC). A strong topological index is expected when a full gap is opened by SOC [18]. Band inversions justify the persistence of surface states in noble metals even in the presence of absorbents such as alkali metals [19–22]. However, these states are generally not robust against backscattering, since there is no symmetry which protects the energy separation between surface and bulk states. This is in clear contrast with topological surface states of band insulators such as Bi_2Se_3 [4]. On the other hand, topologically trivial surface states can arise in quantum wells (thin films) [16], due to band bending in semiconductors [23], or simply from dangling bonds from unbound electrons in semiconductors or insulators [15]. Unlike nontrivial states, trivial states are easily affected, even eliminated, by surface modifications [15,24]. Finally, submonoloayer modifications, such as surface alloying, can lead to a new and (mostly) independent two-dimensional electronic structure resulting in states at the surface as well [25].

Recently, much attention has been drawn to a number of nonsymmorphic materials exhibiting extended linear band dispersions and complex Dirac line nodes, along with extremely large magnetoresistance [26–33]. The most prominent representative is the ternary compound ZrSiS, which has been shown to exhibit an unusual surface electronic structure, which coexists with bulk bands near the Fermi level [26]. Despite various proposals based on

*a.topp@fkf.mpg.de
†raquel.queiroz@weizmann.ac.il

ZrSiS and ZrSnTe [34,35], a quantitative account of the origin and topological character of recurring surface states in this class of compounds still remains unresolved.

In this work, we propose that the surface states of ZrSiS are not derived from the nonsymmorphic bulk band topology, such as hourglass [36] and Dirac [37] surface states, nor are they due to a structural surface modification, but instead are the result of a reduced symmetry at the surface.

As for most nonsymmorphic space groups, the bulk electronic structure of the tetragonal space group $P4/nmm$ (no. 129) is characterized by high band degeneracies (up to fourfold in this case) at certain high symmetry momenta. At the surface, translation symmetry along one direction is broken, and consequently the symmetry is reduced. In the present layered structure, the natural cleavage plane (001) has its symmetry reduced to the symmorphic wallpaper group $P4mm$ (no. 99). Consequently, the high band degeneracies are no longer protected and can be lifted, which can be seen schematically in Fig. 1.

In this regard, the surface states of ZrSiS and related compounds can be seen as "floating" or unpinned two-dimensional surface bands floating on top of the three-dimensional bulk bands, without the need of surface reconstruction. The energy gap separating surface and bulk bands originates from the unpinning of bands along the XM line, as the symmetry enforced degeneracies are locally lifted, but remain pinned in the bulk. Such a symmetry-derived surface electronic structure does not fit any of the aforementioned surface state models, and is not particular to this space group. Without SOC, the spin degeneracy is still preserved in the resulting surface states, so surface floating bands are prone to appear in materials with higher degeneracies (e.g., nonsymmorphic semimetals), which feel a reduced symmetry at the surface.

This article is organized as follows. We present the methods in Sec. II. In Sec. III, we present angle-resolved photoemission spectroscopy (ARPES) data at various photon energies and slab density functional theory (DFT) calculations. In Sec. IV, we show a minimal tight-binding model that qualitatively describes the origin of the floating two-dimensional surface bands. Finally, in Sec. V, we study the sensitivity of the surface bands to surface details by presenting ARPES and DFT calculations of ZrSiS with a monolayer of potassium evaporated on the surface. Our findings are put into perspective of work done on isostructural compounds in Sec. VI.

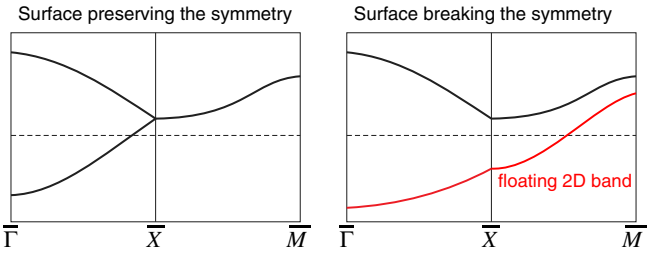

FIG. 1. Schematic of the surface states possible in nonsymmorphic materials, as occurrent in ZrSiS. The symmetry enforcement of the band degeneracy at $\bar{X}$ is relaxed at the surface, creating a sizable energy separation between the surface band (red line) and bulk bands (black lines). With minimal coupling between them, the two-dimensional surface band can be seen as "floating" in an energy region not accessible to bulk states.

II. METHODS

For the ARPES measurements, crystals were cleaved *in situ* and measured in ultrahigh vacuum (low 10^{-10} mbar range). Low-energy ARPES spectra were recorded with the 1^2-ARPES experiment installed at the UE112-PGM2a beam line at BESSY-II. The measurement temperature was 40 K. Soft x-ray ARPES measurements (between $h\nu = 248$ and 1000 eV) were performed at room temperature and 77 K at the 29ID-IEX beam line (Advanced Photon Source, Argonne National Laboratory) using a hemispherical Scienta R4000 electron analyzer with a pass energy of 200 eV (energy and angular resolution are 220 meV and 0.1°, respectively).

For the periodic DFT calculations we employed the Vienna *ab initio* simulation package (VASP) [38] in the framework of the projector augmented wave method. For Zr the $4s$, $4p$, $5s$, and $4d$ were treated as valence states, whereas for S and Si the $3s$, $3p$ states were treated as valence states. For K coating, we employed a projector augmented wave potential that treats the $3s$, $3p$, and $4s$ as valence states. The kinetic energy cutoff for the plane wave basis was set to 500 eV. Unless stated otherwise, we employed the Perdew-Burke-Ernzerhof exchange correlation energy functional. The Brillouin zone (BZ) integrations were carried out using a $4 \times 4 \times 1$ Γ-centered k mesh. The surface model has a slab thickness of 7 unit cells, while the original publication on ZrSiS used a thickness of 5 unit cells [26]. The calculations show no essential difference in comparison. The atomic positions have been kept fixed to the experimental bulk positions. For the adsorption of the K atoms, we have kept the atomic positions of the atoms in the surface fixed, allowing only the K atoms to relax. A coverage of one K atom per surface unit was used and applied to both sides of the slab.

III. SURFACE STATE: ARPES AND DFT

In this section, we present ARPES measurements of the surface state of ZrSiS and show its appearance in a slab DFT calculation. We show a remarkably good correspondence between the two, and present a study of the orbital character of the surface state.

Figure 2(a) shows the experimental band structure of ZrSiS measured at a photon energy of 26 eV. The dispersion is shown along the $\bar{\Gamma}\,\bar{X}\,\bar{M}$ line [the path through the surface BZ is shown in red in Fig. 3(a), while the whole BZ can be seen in Fig. 4(a)]. At the $\bar{X}$ point, the linearly

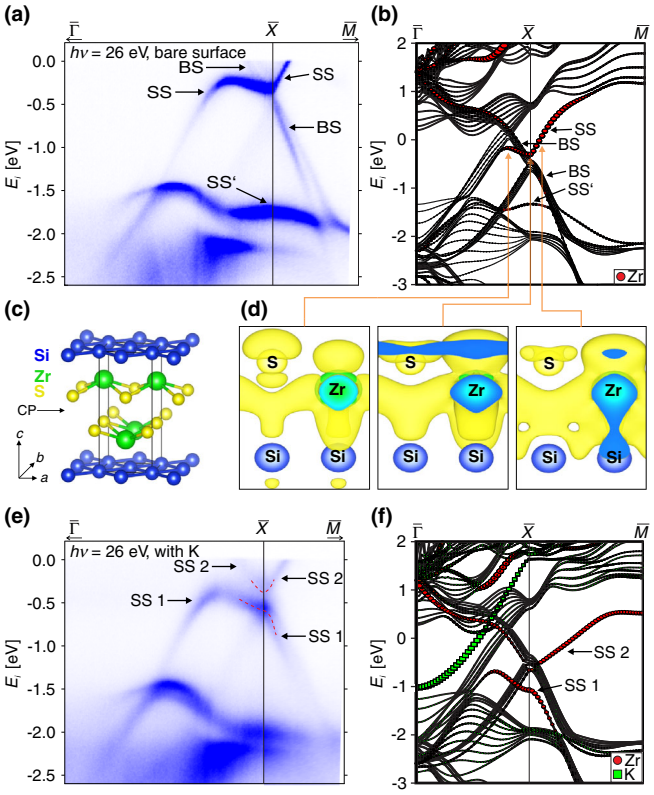

FIG. 2. Visualization of the surface states in ZrSiS. Panels (a) and (b) show dispersion plots along $\overline{\Gamma}\,\overline{X}\,\overline{M}$. The path through the Fermi surface is shown in red in Fig. 3. (a) ARPES data of a bare surface, presenting the surface states (SS and SS′) as high intensity features crossing the bulk bands (BS). (b) DFT slab calculations where the surface state character is indicated by the size of the red circles. (c) Crystal structure of ZrSiS. The unit cell is shown in black. The cleavage plane (*CP*) is indicated by a black arrow. (d) Isosurfaces of the charge density of the surface state at different k points. The arrows indicate the corresponding independent particle states in the band structure. Only the topmost layer of the supercell is shown because the charge density vanishes in the bulk. At the $\overline{X}$ point the surface state is mostly composed of Zr d_{z^2} and S p states. We find that the dispersion of the surface state towards $\overline{\Gamma}$ and $\overline{M}$ is linked to a change in Zr d_{z^2}, d_{xz}, and d_{yz} character. Panels (e) and (f) show dispersion plots along $\overline{\Gamma}\,\overline{X}\,\overline{M}$ for a potassium covered surface. Again, the red circles show the states arising from the surface termination in the calculations. The green squares in (f) show states that originate from an ordered array of potassium atoms on both sides of the slab. In (f), the relaxed z distance between K and the surface is 2.74 Å. The potassium mixes the orbital character of the surface bands, resulting in a gapping of the surface related bands (SS1 and SS2) in (e), which is reproduced, but overestimated, in the DFT calculations. For easier visibility, the red dashed line in (e) shows the band connectivity.

dispersing bulk bands are degenerate at $E_i \approx -0.5$ eV due to the nonsymmorphic symmetry, and continue to lower initial state energies along the $\overline{X}\,\overline{M}$ direction. This bulk band (BS) is intersected by a very intense surface band (SS) just above the nonsymmorphically degenerate point. A second very intense surface band (SS′) is observed at lower initial state energy ($E_i \approx -1.7$ eV). In the following, we focus the discussion on the surface band closer to the Fermi level, labeled SS, although the same arguments hold for the lower surface band. Comparing the experimental results with theoretical calculations in Fig. 2(b), we find good agreement with the dispersion of both surface bands. The surface bands with strong Zr character are highlighted by red circles (larger radius indicates stronger Zr character).

To underline the surface character of the states described above, Fig. 2(d) shows the calculated charge density isosurfaces of the surface state. The isosurface is shown in real space in the first half unit cell below the cleavage plane [indicated by an arrow in Fig. 2(c)]. The extended blue area stems from the inner side of the isosurface, where it cuts the pictured cell. The figure shows that the corresponding independent particle state localizes at the surface and exhibits mostly Zr d_{z^2} and S p character at the $\overline{X}$ point. The dispersion towards $\overline{\Gamma}$ and $\overline{M}$ is linked to a change in its Zr d_{z^2}, d_{xz}, and d_{yz} character. The band character is determined using VASP by calculating the absolute value of the overlap between the respective state and spherical harmonics that are nonzero inside a radius around the considered atomic center [39]. This allows us to measure and plot the surface state character for the present band structure diagrams. A similar statement can be made for the identification of bands with surface character in the case of potassium coated surfaces in Figs. 2(e) and 2(f), which we discuss in Sec. V.

The DFT slab calculations are in an overall agreement with the ARPES data, aside from the energy distance between the nonsymmorphic point and the lower surface band at the $\overline{X}$ point at $E_i = -1.7$ eV in Fig. 2(a), which is underestimated. The very expensive use of a hybrid functional around the $\overline{X}$ point, however, shows that this distance is in fact increasing with the computationally more expensive method.

We performed additional measurements near the $\overline{X}$ point at the APS beam line using higher photon energies. Figure 3(a) shows a comparison of the Fermi surface, measured at Bessy II with 26 eV photons. The red lines indicate the high symmetry directions $\overline{\Gamma}\,\overline{X}$ and $\overline{X}\,\overline{M}$, which correspond to the band dispersions shown in Fig. 2. Figures 3(b)–3(d) show the Fermi surface measured at photon energies of 248, 374, and 700 eV, respectively. All four Fermi surfaces show the diamondlike Dirac nodal loop around the $\overline{\Gamma}$ point and the surface state as a ringlike structure around the $\overline{X}$ point. Note that the surface states are visible for very high photon energies; a cut along $\overline{\Gamma}\,\overline{X}$ in Fig. 3(e) shows them clearly even for 700 eV in the dispersion. The relative intensity of the bulk bands in comparison to the surface states increases, however. This can be explained by the increased inelastic mean-free path of metallic materials from 0.5 nm at 26 eV to 1.4 nm at 700 eV [40]. Since ZrSiS has a high Debye temperature of ≈493 K, this directly increases the intensity of the bulk

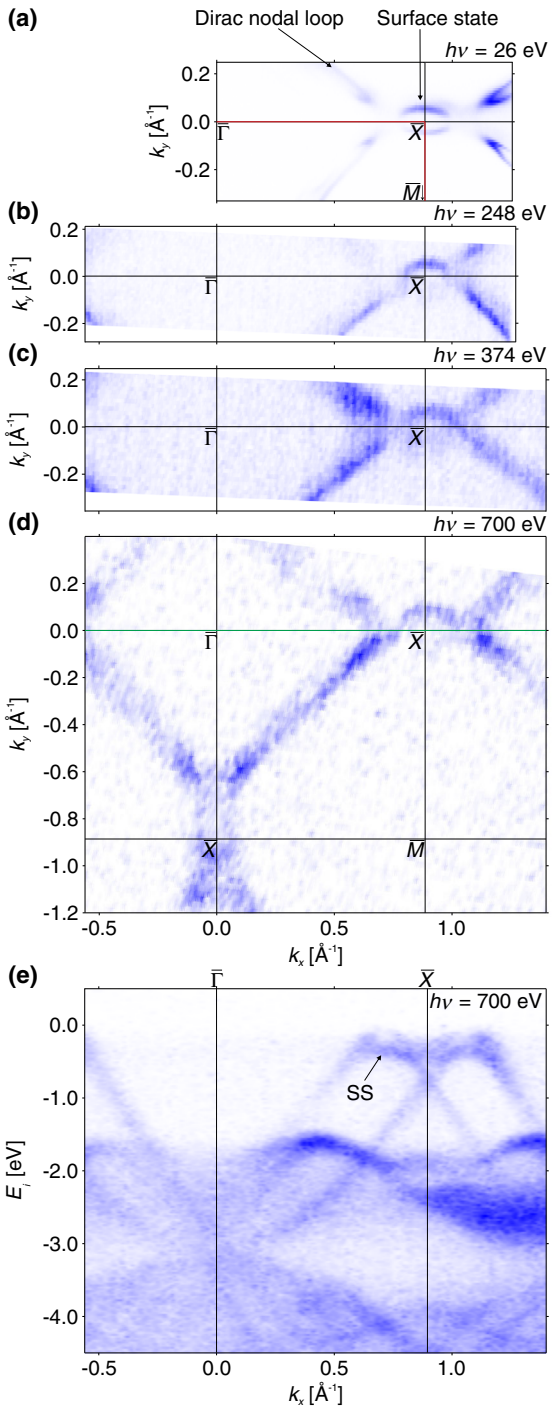

FIG. 3. Constant energy plots at the Fermi level for photon energies (a) $h\nu = 26$ eV, (b) $h\nu = 248$ eV, (c) $h\nu = 374$ eV, and (d) $h\nu = 700$ eV. (a) The bare ZrSiS surface shows the right quadrant of the diamond-shaped Fermi surface as well as the surface-derived pockets around $\overline{X}$. The path for the dispersion data in Fig. 2 is shown in red. Panels (b)–(d) show a similar surface for photon energies of 248, 374, or 700 eV, respectively. (e) Dispersion along $\overline{\Gamma}\,\overline{X}$ for $h\nu = 700$ eV [green line in (d)]. The pockets around $\overline{X}$ are clearly visible in the Fermi surface and the dispersion, showing the considerable weight of these surface states even for high photon energies.

states [41]. The stability of the surface bands against phonon-induced nondirect transmissions could indicate a strong localization of the surface states at the surface [42], which would be expected for surface states caused by a symmetry reduction at the surface.

From the orbital analysis, we conclude that the surface state does not have its origin in a band inversion (because it does not start at a Dirac point). Since it is neither due to surface reconstruction or to alloying [26], as we discuss further below, another reason must be found that explains the relationship between the surface states and the bulk band structure.

IV. SYMMETRIES AND EFFECTIVE MODEL

The matching DFT slab calculations and ARPES measurements confirm the observation of surface states in ZrSiS, but do not reveal their origin. We develop an effective model Hamiltonian that qualitatively reproduces the observed surface density of states. We complement the symmetry discussion and the effective four-band model Hamiltonian with a 26-band tight-binding model fitted to the DFT band structure of ZrSiS. With this model, shown in Fig. 4, we can reproduce faithfully the surface density of states, as observed with ARPES in Fig. 2 and effectively create a link between the model Hamiltonian and the *ab initio* DFT calculations.

Nonsymmorphic symmetries result from spatial transformations where no point is left invariant. They correspond to nontrivial extensions of point group transformations by fractional translations. These are screw axes and glide planes. A nonsymmorphic symmetry matrix representation $\bar{g}_{\boldsymbol{k}}$ is momentum dependent, reflecting that when applied repeatedly it leads to a full lattice translation, not the identity. To avoid cluttering, we omit the momentum index $\boldsymbol{k}$. Nonsymmorphic symmetries are known to create "sticky points" in the electronic band structure [43,44], which are understood as the pinning of complex conjugate symmetry eigenvalues at time-reversal invariant momenta, due to time-reversal symmetry $\mathcal{T}$. A common example of a nonsymmorphic space group is the tetragonal space group no. 129, $P4/nmm$, of which ZrSiS is the a prominent example. It is characterized by a glide plane $\{M_z|\frac{1}{2}\frac{1}{2}0\}$, which is a mirror transformation in $\hat{z}$ and a half-translation along $\hat{x}+\hat{y}$; two screw axes $\{C_{2x}|\frac{1}{2}00\}$ and $\{C_{2y}|0\frac{1}{2}0\}$; a mirror M_{xy}; and inversion $\mathcal{I}$ symmetries. The combination of these symmetries enforces all bands to be degenerate at the X and M points (R and A points) in the bulk BZ, even in the presence of SOC [45]. In the absence of SOC, the enforced degeneracy is extended to the entire XM line. A schematic of the symmetry-protected band degeneracies is shown in Fig. 4(a). Because of the generally small SOC in ZrSiS, we consider spinless electrons in our model. We distinguish the enforced degeneracies (solid color), pinned to specific symmetry invariant momenta,

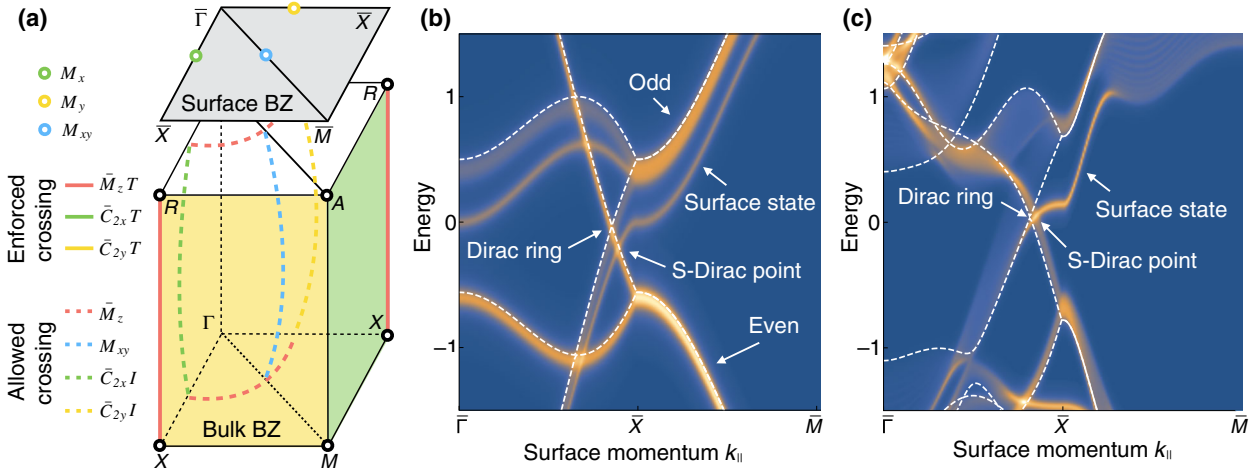

FIG. 4. (a) Schematic of the symmetries of space group $P4/nmm$. Colored planes, lines, and points indicate the symmetry-protected degeneracies in the absence of spin-orbit coupling. Solid colors identify momenta where all states are doubly degenerate due to a combination of a nonsymmorphic symmetry and time reversal; dashed lines represent allowed crossings of bands with different symmetry eigenvalues. At the (001) surface the symmetry is reduced to the symmorphic group $P4mm$. (b) Surface density of states for the effective model in Eqs. (1) and (2), superposed with the bulk band structure at $k_z = 0$ (dashed white line). (c) Surface density of states for a 26-band tight-binding model fitted to the DFT band structure of ZrSiS. The Kramers degeneracy at $\bar{X}$ is lifted at the surface since the symmetry group is reduced to a symmorphic one. This creates a two-dimensional surface band, since the degeneracy at X is lifted. Here, we call such a band floating band. The effect is mostly visible in bands with large k_z dispersion, in contrast to planar orbitals, such as $d_{x^2-y^2}$.

from the crossing of bands with different symmetry eigenvalues along high symmetry planes (dashed lines). The latter are responsible for the observed Dirac rings at $k_z = 0, \pi$ and tubes at $k_x = 0$ and $k_y = 0$ [26]. The former is responsible for the fourfold nonsymmorphic Dirac points at X. We can see representations of both cases in the bulk band structure of ZrSiS as depicted in Fig. 4(c). The states along the XM line are all fourfold degenerate due to the combination of a screw axis and time-reversal symmetries $\bar{C}_{2x}\mathcal{T}$. On the other hand, bands that transform under different eigenvalues of $\bar{C}_{2x}\mathcal{I}$ can cross along the ΓX line. The $k_z = 0$ and $k_z = \pi$ planes, invariant under $\bar{M}_z$, allow for nodal rings as observed in Ref. [26] (partially visible in Fig. 3). The nodal ring is fixed to the Fermi level, as expected from the charge balance in ZrSiS.

So far, the effect of the surface has not yet been taken into account. The crystal cleaves along the (001) plane breaking the translation symmetry along $\hat{z}$. As shown in the previous section, the surface introduces an asymmetry between the two nonsymmorphic sublattices (Zr atoms in the unit cell) due to their displacement along the $\hat{z}$ axis. As a consequence, *all* nonsymmorphic symmetries are broken at the surface. The symmetry group is reduced to the spare wallpaper group $P4mm$ (space group no. 99), which only protects the crossing of surface bands along $\bar{\Gamma}\bar{X}$ and $\bar{\Gamma}\bar{M}$ [see Fig. 4(a), surface BZ]. The remaining symmetry protection of surface bands along the $\bar{\Gamma}\bar{X}$ line can be seen directly in the ARPES data and slab DFT calculations in Figs. 2(a) and 2(b). In fact, from the bulk Dirac ring, only a surface Dirac point remains as $\bar{M}_z$ is broken. Most remarkable is the lifted degeneracy along $\bar{X}\bar{M}$, which is protected in the bulk by the nonsymmorphic symmetries. The additional surface mass terms allow for a drastic gap opening which can detach a surface band from its parent bulk bands, creating a surface floating band.

To qualitatively simulate the band structure, we consider a minimal spinless model without spin-orbit coupling with two sublattices A and B (eigenvalues of the Pauli matrix τ_z), related by a fractional translation along $\hat{x} + \hat{y}$, as well as two orbitals (eigenvalues of σ_z), even and odd with respect to M_z. The band Hamiltonian $\mathcal{H} = \sum_{\boldsymbol{k}} \Phi_{\boldsymbol{k}}^\dagger H_{\boldsymbol{k}} \Phi_{\boldsymbol{k}}$ acts on the basis $\Phi_{\boldsymbol{k}} = |c_{A,+}, c_{A,-}, c_{B,+}, c_{B,-}\rangle_{\boldsymbol{k}}$. Here, $c_{a,i}$ creates an electron in the sublattice $a = A, B$, with orbital $i = +, -$, even or odd under $\bar{M}_z$. Imposing time-reversal and the spatial symmetries, we write the simple hopping Hamiltonian $H_{\boldsymbol{k}} = H_{\boldsymbol{k}}^{\mathrm{s}} + H_{\boldsymbol{k}}^{\mathrm{ns}}$, with a symmorphic component which preserves the sublattice,

$$H_{\boldsymbol{k}}^{\mathrm{s}} = \mu + m\sigma_z + t_{xy}^{\pm}(\cos k_x + \cos k_y)\sigma_{\pm} + t_z^{\pm}\cos k_z \sigma_{\pm}, \qquad (1)$$

for $\sigma_{\pm} = 1 \pm \sigma_z$ the projector into the even (odd) orbital sectors, and a nonsymmorphic part,

$$\begin{aligned} H_{\boldsymbol{k}}^{\mathrm{ns}} = {} & t[1 + \cos k_x + \cos k_y + \cos(k_x + k_y)]\tau_x \\ & + t[\sin k_x + \sin k_y + \sin(k_x + k_y)]\tau_y, \end{aligned} \qquad (2)$$

where the hopping coefficients, coupling the A and B sublattices, are fixed relative to each other [46].

In Fig. 4(b), we show the bulk band structure of $H_{\boldsymbol{k}}$ (white dashed line), together with the surface density of states (color scale) in a slab calculation. We used $\mu = -0.1$, $m = 0.5$, $t_{xy}^{-} = -t_{xy}^{+} = 0.5$, $t_z^{+} = 0.05$, $t_z^{-} = 0.02$, and $t = 0.5$ to qualitatively correspond to the observed band structure in Fig. 2(a).

The surface DOS is calculated following Ref. [47] taking a slab of 20 unit cells. We directly compare the effective model with the DFT-fitted 26-band tight-binding model in Fig. 4(c), where we show the surface density of states. Motivated by the charge density distribution in Fig. 2(d), we expect the surface to create an unbalance between the local chemical potential and hopping amplitudes between the two sublattices. This is expected from the modification in the crystal field at the surface.

We left the even orbital unaffected. This can be justified by the lack of charge density of the bulk band at the cleavage plane, and consequently less sensitivity (or even no sensitivity) to the symmetry reduction at the surface. This is the case in ZrSiS, where the nonsymmorphic Dirac point below the Fermi level retains the bulk symmetry, since it does not occupy the sulfur-p_z orbitals at the surface layer. An explicit depiction of it can be found in Fig. 5, where we show the real space charge density of the bulk states at the X point. In the same figure, we can see that the

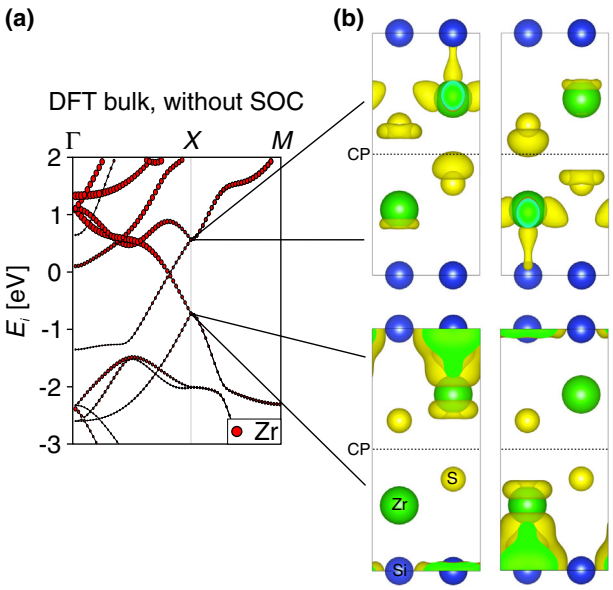

FIG. 5. (a) DFT bulk calculation of ZrSiS. The size of the red colored circles here stands for the overall Zr character in the unit cell, not just of the topmost one, as shown when considering the surface in Figs. 2(b) and 2(f). (b) Orbital character of the bulk bands at the X point shown through the isosurfaces of the charge density. The cleavage plane (CP) is shown as a dashed line in the unit cells. The color scale indicates the affiliation to the atoms (green, Zr; blue, Si; yellow, S). For the ZrSiS bulk material, the conduction band minimum at X shows a considerable DOS in the gap between the sulfur atoms, while the valence band maximum is much less affected by the introduction of a surface.

Dirac point above the Fermi level has a significant sulfur-p_z contribution, which is highly affected by the presence of a surface; see Fig. 2(d). The symmetric orbital, deep in the material, is not affected. This breaks explicitly the symmetry that protects the degeneracy at X, leading to a floating, unpinned, surface band.

We simulate the symmetry reduction, by including a surface potential given by $H^{\mathrm{surf}} = -0.1(\tau_0 + \tau_x)\sigma_+$ at the top and bottom layers. This term breaks the nonsymmorphic symmetry which requires intraband hopping to be equal in the two sublattices.

It is important to note here that the surface in general also breaks inversion symmetry, which can lead to the observation of Rashba splitting of the surface states in related materials like HfSiS [30,48]. In these materials, the Rashba effect spin splits the involved states. This is in addition to the lifting of nonsymmorphic higher degeneracies. Since the involved atoms in ZrSiS are, however, very light, Rashba splitting will not be resolvable. Breaking nonsymmorphic symmetry at the surface, in contrast, has profound influence on the band structure.

V. RESPONSE TO SURFACE MODIFICATION

In the previous sections, we have seen that the surface state results from a symmetry reduction at the surface due to a pronounced orbital deformation in the surface layer. In this context, we investigate how the surface state responds to a local chemical potential modification. For this purpose, we perform additional ARPES measurements with a monolayer of potassium evaporated on the surface.

In Figs. 2(e) and 2(f), we show the ARPES spectrum and DFT slab calculation along $\overline{\Gamma}\,\overline{X}\,\overline{M}$, for a sample with a surface covered with 1 ML potassium. The bulk bands remain nearly unmodified in comparison to the bare surface from Figs. 2(a) and 2(b); only a slight doping effect shifts the energy of the whole band structure. The states with surface character, in contrast, show a clear change. With potassium, the surface state shows a different band connectivity [indicated by the dashed red line in Fig. 2(e)], one part following the bulk bands below the Fermi level along $\overline{X}\,\overline{M}$ (SS1), while its other part going above the Fermi level seems to be connected to a second surface state (SS2). This change in connectivity is additional evidence for the trivial origin of the surface state. The observed changes under potassium coating can be reproduced by performing DFT slab calculations of a surface covered with a regular array of potassium atoms. The results for a relaxed K distance of 2.74 Å from the surface are shown in Fig. 2(f). Again, we see very good agreement between theory and experiment. The two surface states, SS1 and SS2, which where connected previously [SS in Figs. 2(a) and 2(b)], are now gapped and connected to a band that roughly follows the bulk bands. In Fig. 2(b), this band already showed a similar orbital character as the surface state above, but not at the Fermi level, illustrated by the red circles. Without

potassium, these states do not interfere and the surface state is crossing all bulk bands just above the nonsymmorphically protected point. With potassium, however, this band shows surface state character at the Fermi level leading to a gapping of the former crossing.

In that context it makes sense to analyze the orbital character in more detail to understand the change in the floating 2D band with potassium. As explained in the previous theory section, the bands have different orbital character, allowing them to cross along the $\overline{\Gamma}\,\overline{X}$ line. The potassium mixes their orbital character; therefore, we observe an avoided crossing and a different band connectivity. This avoided crossing is also expected in the presence of spin-orbit coupling, as presented in Ref. [26]. However, since SOC is very weak in ZrSiS, the gap is visible only when the surface potential is varied by the potassium.

This prediction from the tight-binding model is very well caught in the DFT calculations in Fig. 2(f). However, ARPES does not capture the states that are presented in green in the DFT calculations. This is because they arise from a hypothetical regular array of potassium, which is not present in reality when evaporated at temperatures of 40 K. Furthermore, we note that structural relaxation effects for the adsorbed K layer are another possible source for the discrepancy between DFT and ARPES experiments. Figure 2(f) shows calculations for a relaxed K atom distance. The gap at the $\overline{X}$ point, between the surface states SS1 and SS2, is very pronounced and the change in the band connectivity is obvious. Nevertheless, this does not represent the measurements, where the gap is very small and the lower surface band even lies in the bulk bands. When increasing the distance of potassium atoms from the surface manually, the lower surface band shifts up, since the mixing in orbital character is reduced again. This implies a strong dependence of the DFT results on the modified surface potential agreeing with the fact that in the limit of a very large distance, a crossing is allowed again and the original band connectivity is restored. The overestimation of the gap in the DFT calculations can have different reasons. Firstly, a coverage of 1 ML is experimentally not possible. In reality, an error of up to 10% is not unlikely. A partial monolayer or a partial bilayer coverage of potassium might very well show a different relaxed distance from the surface. Secondly, the DFT calculation itself might overestimate the effect of the regular potassium layer on the surface. More accurate, beyond DFT approaches for the calculation of the band structure could provide additional insight and even better agreement with experiment. However, such methods are, due to their relatively large computational cost and the required system size for the surface model, currently not applicable.

VI. DISCUSSION AND CONCLUSION

We find that the origin of the surface states in ZrSiS and related compounds can be attributed to the symmetry reduction at the surface. This could be modeled by locally breaking the nonsymmorphic glide plane symmetry, introducing a large mass for the S-p_z and Zr-$(d_{xz}+d_{yz})$ orbitals, which leads to a floating two-dimensional band close to the Fermi level.

Here, we discuss these results in the light of previous, alternative explanations for the surface states in ZrSiS-type materials.

One might be tempted to think that the surface state is a result of the band inversion at the Fermi level that is gapped by a small amount by SOC. If this were to cause a topological nontrivial gap, topological surface states are expected [34]. ZrSiS, however, shows a $\mathbb{Z}_2$ invariant of 0(001) (analogous to ZrSiO [31]), i.e., it is a weak topological insulator, which implies that there are no topological surface states expected on the (001) surface [49]. In this paper, we show that the surface states can be fully explained not involving topology, thus clarifying that surfaces states can appear due to trivial reasons in nonsymmorphic materials.

Another possibility for surface states could be dangling bonds, resulting from the Zr atoms that might have been bonded weakly to a sulfur atom from the next nearest S layer above. Such dangling bonds would be expected to be saturated by potassium evaporation, however. Potassium coating would be expected to modify these states much more strongly than what is observed here [50,51]. Furthermore, in contrast to what was found in ZrSnTe, we do not observe any sign of hydrogenation in ZrSiS within much longer time scales than studied in ZrSnTe [35]. We can therefore rule out the presence of dangling bonds in cleaved ZrSiS.

Lastly, it was proposed that surface states in ZnSnTe could be explained by a freestanding monolayer on the surface of the bulk [35], which was supported by monolayer DFT and slab calculations. A monolayer preserves the nonsymmorphic symmetries and inversion symmetry, while a slab calculation breaks both at the surface. Therefore, they lead to completely different behavior at the X point. In a monolayer all bands are still fourfold degenerate, as explicitly shown by Guan *et al.* on a monolayer HfGeTe [52] (isostructural to ZrSiS). A slab calculation, which models the surface more appropriately, shows that the surface bands are only doubly degenerate, while the bulk bands remain fourfold degenerate at X, describing the exact behavior we observe in ZrSiS.

Because of the general symmetry arguments in our model, we conclude that similar surface floating bands are expected to appear in other layered nonsymmorphic compounds. Since a symmetry reduction at the surface lifts the degeneracy in the bulk band structure, materials with such "sticky points" are prone to show these states. In particular, other compounds from space group 129 are very likely to show them and indeed, e.g., in ZrSiTe or HfSiS such unexpected surface states could have already been found [29,30].

This does not necessarily imply that all degeneracies at high symmetry points are automatically lifted at the surface. In fact, the ARPES data in Fig. 2(a), as well as the tight-binding model in Fig. 4(c), show that only the upper degenerate point at $\overline{X}$ is lifted, due to its orbital character and sufficient density of states in the cleavage plane. This behavior has to be taken into account before applying this phenomenon to every nonsymmorphic degeneracy in the band structure of ZrSiS and related materials.

Furthermore, we show the peculiar properties of the surface states in question. They prevail for high photon energies up to 700 eV and are prone to gapping around the $\overline{X}$ point when covered with a monolayer of potassium, mixing the orbital characters of the states in question. The weak coupling between surface and bulk bands due to a large, symmetry-induced, energy separation makes the surface state highly two dimensional and susceptible to surface potentials. The surface bands' low energy excitations behave as effective two-dimensional electrons, floating on top of the three-dimensional bulk, with properties dictated by the reduced symmetry group at the surface.

ACKNOWLEDGMENTS

The authors thank Benjamin Balke for inspiring discussions and his insight into the matter of surface states. L. M. would like to thank Yang Zhang for providing the tight-binding parameters. Work at Argonne National Laboratory is supported by the U.S. Department of Energy, Office of Science, under Contract No. DE-AC02-06CH11357; additional support by National Science Foundation under Grant No. DMR-0703406. We thank HZB for the allocation of synchrotron radiation beamtime. This work was partially supported by the DFG, proposal no. SCHO 1730/1-1.

[1] C. L. Kane and E. J. Mele, *Quantum Spin Hall Effect in Graphene*, Phys. Rev. Lett. **95**, 226801 (2005).

[2] L. Fu, C. L. Kane, and E. J. Mele, *Topological Insulators in Three Dimensions*, Phys. Rev. Lett. **98**, 106803 (2007).

[3] A. P. Schnyder, S. Ryu, A. Furusaki, and A. W. W. Ludwig, *Classification of Topological Insulators and Superconductors in Three Spatial Dimensions*, Phys. Rev. B **78**, 195125 (2008).

[4] H. Zhang, C.-X. Liu, X.-L. Qi, X. Dai, Z. Fang, and S.-C. Zhang, *Topological Insulators in* Bi_2Se_3, Bi_2Te_3 *and* Sb_2Te_3 *with a Single Dirac Cone on the Surface*, Nat. Phys. **5**, 438 (2009).

[5] Y. Ando, *Topological Insulator Materials*, J. Phys. Soc. Jpn. **82**, 102001 (2013).

[6] *The Nobel Prize in Physics 2016*, www.nobelprize.org/nobel_prizes/physics/laureates/2016/, accessed April 25, 2017.

[7] X. Wan, A. M. Turner, A. Vishwanath, and S. Y. Savrasov, *Topological Semimetal and Fermi-Arc Surface States in the Electronic Structure of Pyrochlore Iridates*, Phys. Rev. B **83**, 205101 (2011).

[8] B. Yan and S.-C. Zhang, *Topological Materials*, Rep. Prog. Phys. **75**, 096501 (2012).

[9] C. Fang, M. J. Gilbert, X. Dai, and B. A. Bernevig, *Multi-Weyl Topological Semimetals Stabilized by Point Group Symmetry*, Phys. Rev. Lett. **108**, 266802 (2012).

[10] C.-K. Chiu and A. P. Schnyder, *Classification of Reflection-Symmetry-Protected Topological Semimetals and Nodal Superconductors*, Phys. Rev. B **90**, 205136 (2014).

[11] Z. K. Liu, B. Zhou, Y. Zhang, Z. J. Wang, H. M. Weng, D. Prabhakaran, S.-K. Mo, Z. X. Shen, Z. Fang, X. Dai, Z. Hussain, and Y. L. Chen, *Discovery of a Three-Dimensional Topological Dirac Semimetal,* Na_3Bi, Science **343**, 864 (2014).

[12] Z. K. Liu, J. Jiang, B. B. Zhou, Z. J. Wang, Y. Zhang, H. M. Weng, D. Prabhakaran, S.-K. Mo, H. Peng, P. Dudin, T. Kim, M. Hoesch, Z. Fang, X. Dai, Z.-X. X. Shen, D. L. Feng, Z. Hussain, and Y. Chen, *A Stable Three-Dimensional Topological Dirac Semimetal* Cd_3As_2, Nat. Mater. **13**, 677 (2014).

[13] C. Shekhar, A. K. Nayak, Y. Sun, M. Schmidt, M. Nicklas, I. Leermakers, U. Zeitler, Y. Skourski, J. Wosnitza, Z. Liu, Y. Chen, W. Schnelle, H. Borrmann, Y. Grin, C. Felser, and B. Yan, *Extremely Large Magnetoresistance and Ultrahigh Mobility in the Topological Weyl Semimetal Candidate NbP*, Nat. Phys. **11**, 645 (2015).

[14] Y.-H. Chan, C.-K. Chiu, M. Y. Chou, and A. P. Schnyder, Ca_3P_2 *and Other Topological Semimetals with Line Nodes and Drumhead Surface States*, Phys. Rev. B **93**, 205132 (2016).

[15] J. E. Northrup, *Origin of Surface States on* $Si(111)(7 \times 7)$, Phys. Rev. Lett. **57**, 154 (1986).

[16] J. Paggel, T. Miller, and T.-C. Chiang, *Quantum-Well States as Fabry-Pérot Modes in a Thin-Film Electron Interferometer*, Science **283**, 1709 (1999).

[17] S. G. Davison and M. Steslicka, *Basic Theory of Surface States*, revised edition (Clarendon Press, Oxford, 1992).

[18] B. Yan, B. Stadtmüller, N. Haag, S. Jakobs, J. Seidel, D. Jungkenn, S. Mathias, M. Cinchetti, M. Aeschlimann, and C. Felser, *Topological States on the Gold Surface*, Nat. Commun. **6**, 10167 (2015).

[19] S. Lindgren and L. Walldén, *Energy Shifts of a Cu(111) Surface Band Upon Adsorption of Cesium and Oxygen*, Surf. Sci. **89**, 319 (1979).

[20] D. Tang, C. Su, and D. Heskett, *The Unoccupied Electronic Structure of Na/Cu(110)*, Surf. Sci. **295**, 427 (1993).

[21] S. D. Kevan and R. H. Gaylord, *Anomalous Surface-State Penetration Near a Band Edge*, Phys. Rev. Lett. **57**, 2975 (1986).

[22] P. Sandl and E. Bertel, *Surface States, Local Bonding, and Surface Reconstruction: Na on Cu(110)*, Surf. Sci. **302**, L325 (1994).

[23] H. M. Benia, C. Lin, K. Kern, and C. R. Ast, *Reactive Chemical Doping of the* Bi_2Se_3 *Topological Insulator*, Phys. Rev. Lett. **107**, 177602 (2011).

[24] E. Cartier, J. Stathis, and D. Buchanan, *Passivation and Depassivation of Silicon Dangling Bonds at the* Si/SiO_2 *Interface by Atomic Hydrogen*, Appl. Phys. Lett. **63**, 1510 (1993).

[25] C. R. Ast, J. Henk, A. Ernst, L. Moreschini, M. C. Falub, D. Pacilé, P. Bruno, K. Kern, and M. Grioni, *Giant Spin*

Splitting through Surface Alloying, Phys. Rev. Lett. **98**, 186807 (2007).

[26] L. M. Schoop, M. N. Ali, C. Straßer, A. Topp, A. Varykhalov, D. Marchenko, V. Duppel, S. Parkin, B. V. Lotsch, and C. R. Ast, *Dirac Cone Protected by Non-Symmorphic Symmetry and Three-Dimensional Dirac Line Node in ZrSiS*, Nat. Commun. **7**, 11696 (2016).

[27] Y.-Y. Lv, B.-B. Zhang, X. Li, S.-H. Yao, Y. Chen, J. Zhou, S.-T. Zhang, M.-H. Lu, and Y.-F. Chen, *Extremely Large and Significantly Anisotropic Magnetoresistance in ZrSiS Single Crystals*, Appl. Phys. Lett. **108**, 244101 (2016).

[28] M. N. Ali, L. M. Schoop, C. Garg, J. M. Lippmann, E. Lara, B. Lotsch, and S. S. Parkin, *Butterfly Magnetoresistance, Quasi-2D Dirac Fermi Surface and Topological Phase Transition in ZrSiS*, Sci. Adv. **2**, e1601742 (2016).

[29] A. Topp, J. M. Lippmann, A. Varykhalov, V. Duppel, B. V. Lotsch, C. R. Ast, and L. M. Schoop, *Non-Symmorphic Band Degeneracy at the Fermi Level in ZrSiTe*, New J. Phys. **18**, 125014 (2016).

[30] D. Takane, Z. Wang, S. Souma, K. Nakayama, C. X. Trang, T. Sato, T. Takahashi, and Y. Ando, *Dirac-Node Arc in the Topological Line-Node Semimetal HfSiS*, Phys. Rev. B **94**, 121108 (2016).

[31] Q. Xu, Z. Song, S. Nie, H. Weng, Z. Fang, and X. Dai, *Two-Dimensional Oxide Topological Insulator with Iron-Pnictide Superconductor LiFeAs Structure*, Phys. Rev. B **92**, 205310 (2015).

[32] X. Wang, X. Pan, M. Gao, J. Yu, J. Jiang, J. Zhang, H. Zuo, M. Zhang, Z. Wei, W. Niu *et al.*, *Evidence of Both Surface and Bulk Dirac Bands and Anisotropic Nonsaturating Magnetoresistance in ZrSiS*, Adv. Electron. Mater. **2**, 1600228 (2016).

[33] J. Zhang, M. Gao, J. Zhang, X. Wang, X. Zhang, M. Zhang, W. Niu, R. Zhang, and Y. Xu, *Transport Evidence of 3D Topological Nodal-Line Semimetal Phase in ZrSiS*, Front. Phys. **13**, 137201 (2018).

[34] M. Neupane, I. Belopolski, M. M. Hosen, D. S. Sanchez, R. Sankar, M. Szlawska, S.-Y. Xu, K. Dimitri, N. Dhakal, P. Maldonado, P. M. Oppeneer, D. Kaczorowski, F. Chou, M. Z. Hasan, and T. Durakiewicz, *Observation of Topological Nodal Fermion Semimetal Phase in ZrSiS*, Phys. Rev. B **93**, 201104 (2016).

[35] R. Lou, J.-Z. Ma, Q.-N. Xu, B.-B. Fu, L.-Y. Kong, Y.-G. Shi, P. Richard, H.-M. Weng, Z. Fang, S.-S. Sun *et al.*, *Emergence of Topological Bands on the Surface of ZrSnTe Crystal*, Phys. Rev. B **93**, 241104 (2016).

[36] Z. Wang, A. Alexandradinata, R. Cava, and B. A. Bernevig, *Hourglass Fermions*, Nature (London) **532**, 189 (2016).

[37] B. J. Wieder, B. Bradlyn, Z. Wang, J. Cano, Y. Kim, H.-S. D. Kim, A. Rappe, C. Kane, and B. A. Bernevig, *Wallpaper Fermions and the Topological Dirac Insulator*, arXiv:1705.01617.

[38] G. Kresse and D. Joubert, *From Ultrasoft Pseudopotentials to the Projector Augmented-Wave Method*, Phys. Rev. B **59**, 1758 (1999).

[39] See the VASP manual, www.vasp.at.

[40] M. P. Seah and W. Dench, *Quantitative Electron Spectroscopy of Surfaces: A Standard Data Base for Electron Inelastic Mean Free Paths in Solids*, Surf. Interface Anal. **1**, 2 (1979).

[41] R. Sankar, G. Peramaiyan, I. P. Muthuselvam, C. J. Butler, K. Dimitri, M. Neupane, G. N. Rao, M.-T. Lin, and F. Chou, *Crystal Growth of Dirac Semimetal ZrSiS with High Magnetoresistance and Mobility*, Sci. Rep. **7**, 40603 (2017).

[42] P. Hofmann, C. Søndergaard, S. Agergaard, S. V. Hoffmann, J. E. Gayone, G. Zampieri, S. Lizzit, and A. Baraldi, *Unexpected Surface Sensitivity at High Energies in Angle-Resolved Photoemission*, Phys. Rev. B **66**, 245422 (2002).

[43] L. Michel and J. Zak, *Connectivity of Energy Bands in Crystals*, Phys. Rev. B **59**, 5998 (1999).

[44] C. J. Bradley and A. Cracknell, *The Mathematical Theory of Symmetry in Solids* (Clarendon Press, Oxford; Oxford University Press, New York, 2010).

[45] S. M. Young and C. L. Kane, *Dirac Semimetals in Two Dimensions*, Phys. Rev. Lett. **115**, 126803 (2015).

[46] Y. X. Zhao and A. P. Schnyder, *Nonsymmorphic Symmetry-Required Band Crossings in Topological Semimetals*, Phys. Rev. B **94**, 195109 (2016).

[47] R. Queiroz and A. P. Schnyder, *Helical Majorana Surface States of Strongly Disordered Topological Superconductors with Time-Reversal Symmetry*, Phys. Rev. B **91**, 014202 (2015).

[48] C. Chen, X. Xu, J. Jiang, S.-C. Wu, Y. Qi, L. Yang, M. Wang, Y. Sun, N. Schröter, H. Yang *et al.*, *Dirac Line Nodes and Effect of Spin-Orbit Coupling in the Nonsymmorphic Critical Semimetals MSiS (*M = Hf*, Zr)*, Phys. Rev. B **95**, 125126 (2017).

[49] C. Pauly, B. Rasche, K. Koepernik, M. Richter, S. Borisenko, M. Liebmann, M. Ruck, J. van den Brink, and M. Morgenstern, *Electronic Structure of the Dark Surface of the Weak Topological Insulator* $Bi_{14}Rh_3I_9$, ACS Nano **10**, 3995 (2016).

[50] Y. Sun, S.-C. Wu, and B. Yan, *Topological Surface States and Fermi Arcs of the Noncentrosymmetric Weyl Semimetals TaAs, TaP, NbAs, and NbP*, Phys. Rev. B **92**, 115428 (2015).

[51] M. Tao, D. Udeshi, N. Basit, E. Maldonado, and W. P. Kirk, *Removal of Dangling Bonds and Surface States on Silicon (001) with a Monolayer of Selenium*, Appl. Phys. Lett. **82**, 1559 (2003).

[52] S. Guan, Y. Liu, Z.-M. Yu, S.-S. Wang, Y. Yao, and S. A. Yang, *Two-Dimensional Spin-Orbit Dirac Point in Monolayer HfGeTe*, Phys. Rev. Mater. **1**, 054003 (2017).